



Controlled temperature-mediated curcumin release from magneto-thermal nanocarriers to kill bone tumors

A. Khodaei^{a,b,*}, F. Jahanmard^b, H.R. Madaah Hosseini^{c,**}, R. Bagheri^c, A. Dabbagh^d,
H. Weinans^b, S. Amin Yavari^{b,e}

^a Institute for Nanoscience and Nanotechnology, Sharif University of Technology, Tehran, Iran

^b Department of Orthopedics, University Medical Center Utrecht, Utrecht, the Netherlands

^c Department of Materials Science and Engineering, Sharif University of Technology, Tehran, Iran

^d School of Medicine, Faculty of Health and Medical Sciences, Taylor's University, Subang Jaya, Malaysia

^e Regenerative Medicine Utrecht, Utrecht University, Utrecht, the Netherlands

ARTICLE INFO

Keywords:

Osteosarcoma
Magnetic hyperthermia
Curcumin
MRI contrast agent

ABSTRACT

Systemic chemotherapy has lost its position to treat cancer over the past years mainly due to drug resistance, side effects, and limited survival ratio. Among a plethora of local drug delivery systems to solve this issue, the combinatorial strategy of chemo-hyperthermia has recently received attention. Herein we developed a magneto-thermal nanocarrier consisted of superparamagnetic iron oxide nanoparticles (SPIONs) coated by a blend formulation of a three-block copolymer Pluronic F127 and F68 on the oleic acid (OA) in which Curcumin as a natural and chemical anti-cancer agent was loaded. The subsequent nanocarrier SPION@OA-F127/F68-Cur was designed with a controlled gelation temperature of the shell, which could consequently control the release of curcumin. The release was systematically studied as a function of temperature and pH, via response surface methodology (RSM). The bone tumor killing efficacy of the released curcumin from the carrier in combination with the hyperthermia was studied on MG-63 osteosarcoma cells through Alamar blue assay, live-dead staining and apoptosis caspase 3/7 activation kit. It was found that the shrinkage of the F127/F68 layer stimulated by elevated temperature in an alternative magnetic field caused the curcumin release. Although the maximum release concentration and cell death took place at 45 °C, treatment at 41 °C was chosen as the optimum condition due to considerable cell apoptosis and lower side effects of mild hyperthermia. The cell metabolic activity results confirmed the synergistic effects of curcumin and hyperthermia in killing MG-63 osteosarcoma cells.

1. Introduction

Bone tumors, arising both at a young age and adulthood, can significantly reduce the life span and quality of patients [1]. Osteosarcoma (OS) is the most common mesenchymal origin bone tumor [2], and since nearly 80% of diagnosed cases of OS are in the metastatic stage, pre and post-operative chemotherapy are crucial [3,4]. On the other hand, the most efficacious chemotherapeutic agents for OS treatment, such as cisplatin and doxorubicin, can improve patient survival ratio in 5 years, yet they can only reach a plateau up to 70% due to the drug resistance [5]. This necessitated the use of combinatorial strategies composed of both chemical and physical treatments such as

chemo-photodynamic and chemo-hyperthermia with an on-demand release system to minimize the side-effects [5,6]. Drug resistance and undesirable side-effects of conventional chemotherapeutic agents highlight the role of new natural derived products for cancer treatment [7]. Curcumin as a natural herb has been considered as an anti-cancer chemical specifically for osteosarcoma therapy by inhibiting NF- κ B protein and inducing cell apoptosis [8–11]. Curcumin was also used as a photoinitiator in photodynamic therapy (PDT) using UV-Vis spectrum, which made it an interesting option for combined cancer therapy [12, 13]. Due to the hydrophobicity of curcumin, developing long blood circulating hydrophilic carriers to encapsulate and provide release of sufficient dosage should be seriously considered. Smart nanocarriers that are stimuli-responsive would enhance the site-specific release and

Peer review under responsibility of KeAi Communications Co., Ltd.

* Corresponding author. Institute for Nanoscience and Nanotechnology, Sharif University of Technology, Tehran, 14588, Iran.

** Corresponding author. Department of Materials Science and Engineering, Sharif University of Technology, Tehran, 14588, Iran.

E-mail addresses: a.khodaei-2@umcutrecht.nl (A. Khodaei), madaah@sharif.edu (H.R. Madaah Hosseini), s.aminyavari@umcutrecht.nl (S. Amin Yavari).

<https://doi.org/10.1016/j.bioactmat.2021.09.028>

Received 12 March 2021; Received in revised form 11 August 2021; Accepted 23 September 2021

Available online 5 October 2021

2452-199X/© 2021 The Authors. Publishing services by Elsevier B.V. on behalf of KeAi Communications Co. Ltd. This is an open access article under the CC

BY-NC-ND license (<http://creativecommons.org/licenses/by-nc-nd/4.0/>).

Abbreviations

(SPION)	Superparamagnetic iron oxide nanoparticle
(OA)	Oleic acid
(RSM)	Response surface methodology
(OS)	Osteosarcoma
(PDT)	Photodynamic therapy
(LCST)	Lower critical solution temperature
(TEM)	Transmission Electron Microscopy
(FTIR)	Fourier-transform infrared spectroscopy
(VSM)	Vibrating sample magnetometer
(DLS)	Dynamic light scattering

(CCD)	Central Composite Design
(DMEM)	Dulbecco's Modified Eagle Medium
(CSLM)	Confocal laser microscope
(AMF)	Alternative magnetic field
(SPA)	Specific power absorption
(SAR)	Specific absorption rate
(ANOVA)	Analysis of variance
(PDI)	Polydispersity index
(MAR)	Motional-averaging regime
(ELR)	Echo-limiting regime
(BF)	Bright-field

decrease the cytotoxicity as well [14]. Electromagnetically triggered nanocarriers are promising candidates for this purpose since the human body is mostly transparent to magnetic fields [15]. Moreover, they are considered as negative MRI contrast agents to verify the cancer treatment efficacy [16].

SPION is the most common biocompatible magnetic core for switchable magnetic hyperthermia and magnetically controlled drug delivery systems, which allows tumor-targeting via an external magnetic field [17,18]. Despite the design of different coatings and surface modifications on SPIONs to yield a smart anti-cancer drug delivery, such controlled drug delivery system in the colloidal phase has been rarely explored [19–21]. On the other hand, several magnetic carriers have been introduced to locally deliver curcumin, but they are limited to complex multilayer structures and triggered only via mechanical forces [22,23]. Pluronic is a nonionic three-block copolymer composed of a central hydrophobic chain of polyoxypropylene flanked by hydrophilic polyoxyethylene (PEO-PPO-PEO) that can be used as the carrier of hydrophobic drugs that interact with the hydrophobic PPO block [24]. Pluronic has also been recognized as a long-circulating, anti-metastases and anti-chemoresistance agent thanks to its strong effect on changing tumor viscosity and inhibiting multiple drug-resistant proteins [25–28]. Although pH-responsive curcumin release systems based on pluronic have been studied before, its thermo-responsive behavior is remained relatively unexplored [29].

Although magnetic hyperthermia was introduced in 1957 by Gilchrist et al. and used for clinical application in Europe for brain tumor targeting since 2004 [30] it has not been extensively used yet mainly due to inducing eddy current and heating of healthy tissues within the sufficient frequency and currents ranges [31]. Thus, combining “mild hyperthermia” [32] with controlled release of novel drugs to provide a synergistic effect in the eradication of the tumor cells should be seriously considered. In our previous work [33] we have reported the blend formulation of Pluronic F127, and F68 on the oleic acid coated SPION to model lower critical solution temperature (LCST), however the release study and optimization of the electromagnetic field according to its bio-functionality were remained unexplored [33]. Here, we used the aforementioned nanocarrier for curcumin delivery triggered by mild hyperthermia. The parallel effect of temperature and pH on the concentration of released curcumin was systematically studied using Response Surface Methodology (RSM) for the first time. Furthermore, the potential of this system as a synergistic chemo-hyperthermia osteosarcoma therapy was studied *in vitro*.

2. Materials and methods

2.1. Synthesis of SPION@OA-F127/F68-Cur (CurLNC)

According to the previously extracted model by our group, the parameters in the synthesis protocol of magnetic nanocarriers were selected to adjust the LCST around 45 °C [33]. Coating of nanoparticles

was applied using 14.5 ml oleic acid (Sigma) per gram of particles, polymer/particle ratio of 12.5, and F127/F68 (Sigma) ratio of 1.5. These particles were recognized as nanocarriers (NCs). Loading of curcumin (Sigma) was applied similar to the previously used method [21]. In this process, curcumin was dissolved in acetone (10 mg/ml), and the solution was added dropwise to the deionized water dispersed NCs (200 µl/10 mg) while the particles had a concentration of 10 mg/3 ml water. To enhance the loading efficiency, the colloid was stirred at 0 °C for 2 h, and it was kept overnight at room temperature. Low temperature increases the hydrophilicity, expands the molecules of pluronic, and simplifies the diffusion and absorption of curcumin in the hydrophobic parts of the NCs. Bare SPION, NC, and CurLNC as three experimental groups were used for further studies.

2.2. Materials characterization

The Transmission Electron Microscopy (TEM- LEO Libra 120 kV, Carl Zeis AG) was used to determine the particle size and morphology. The Image J software was used to display particles size histogram through analyzing TEM images. The Fourier-transform infrared spectroscopy (FTIR- MB-100, ABB Bomem) was conducted to show the absorption of the polymers on the surface of the magnetite core and curcumin on the hydrophobic parts of pluronic. In this regard, the samples were mixed with potassium bromide and were packed to make transparent pellets. The vibrating sample magnetometer (VSM- Meghnatis Daghigh Kavir) was used to determine the magnetic properties of the three group samples. Dynamic light scattering (DLS- Malvern Nano S) was used to determine the hydrodynamic diameter of the particles. Polydispersity index (PDI) of single particle size was extracted from TEM micrographs and calculated according to equation (1). Where SD is standard deviation, σ is the average diameter and particles with $PDI < 0.1$ were considered as monodispersed [34]. A zeta-sizer 7.11 (Malvern instruments) was used to measure the nanoparticles surface charge at pH = 7.

$$PDI = \left(\frac{SD}{\sigma}\right)^2 \quad (1)$$

For studying the hyperthermia properties of the samples, a magnetic hyperthermia setup (Easy heat 3542LI, 4 kW, Ambrell, Gloucestershire, UK) with eight coil spirals (2.54 cm diameter) was used. The dried samples with the concentration of 1 mg/ml were dispersed in thermo-sensitive tissue-mimicking phantom to simulate the body condition [35,36]. Table 1 described the used parameters of Alternative magnetic field (AMF) in the hyperthermia setup. The frequency of the oscillations was adjusted in the range of 310–330 kHz. The magnetic field strength (H) was calculated in each condition, considering equation (2). Where n, i, and L represent the coil turns, current (A), and inner coil diameter (m). The heating efficiency of samples was quantified by calculating specific absorption rate (SAR) according to equation (3). C is the specific heat capacity of colloid which can be calculated as $C = (C_{medium} \times m_{medium}) +$

Table 1

The applied parameters of AMF to determine heating efficiency of nanoparticles.

Condition	Current (A)	Frequency (kHz)	Power (W)	Magnetic field (kA. m ⁻¹)
1	50.4	326	0–4	15.74
2	100.8	318	77–92	31.49
3	151.2	313	327–351	47.24
4	201.6	312	717–738	62.99
5	249.9	311	1279–1360	78.74
6	300.3	311	2028–2184	94.01

($C_{SPIONs} \times m_{SPIONs}$). specific heat capacity for medium and SPIONs was considered equal to $4.18 \text{ J g}^{-1} \text{ }^{\circ}\text{C}^{-1}$ and $0.65 \text{ J g}^{-1} \text{ }^{\circ}\text{C}^{-1}$. m_{medium} and m_{SPIONs} also represents partial mass of each component in the colloidal dispersion with concentration of 1 mg/ml. m_{Fe} also indicates the iron mass per unit of SPIONs mass. Moreover, $\frac{dT}{dt}$ was extracted as the slope of temperature-time profiles in the linear area of 0–120s [37].

$$H = \frac{ni}{L} \quad (2)$$

$$SAR = \left(\frac{C}{m_{Fe}}\right) \left(\frac{dT}{dt}\right) \quad (3)$$

2.3. Curcumin release study using RSM

The RSM/Central Composite Design (CCD) was used to design the experiments and model the concentration of the released drug from CurLNCs. The release concentration was studied as a function of pH and temperature (Table 2). In this design, the center point run was replicated six times to assess the error. The loading capacity, loading efficiency (equations (4) and (5)), and concentration of released curcumin were determined using UV–Vis spectroscopy. In particular, 2 ml of colloidal samples (1 mg/ml) were placed in 5 ml glass containers, and the bain-marie water bath was used to provide the required temperature. After 1 h of incubation, the particles were collected using an Nd–Fe–B permanent magnet. The remained carriers were collected and washed with 2 ml water. In the following, they were dispersed in 2 ml acetone to extract the remained drug. The colloid was agitated in an ultrasound bath for 2 min and the supernatant was collected and analyzed using UV–Vis spectroscopy. The released concentration was indirectly calculated based on reminded drug concentration.

$$\text{Loading Capacity} = \frac{\text{Loaded drug weight}}{\text{Particle weight}} \times 100 \quad (4)$$

$$\text{Loading efficiency} = \frac{\text{Loaded drug weight}}{\text{total drug weight}} \times 100 \quad (5)$$

2.4. Relaxometry

To analyse the r_1 and r_2 relaxivity of the nanoparticles, MRI phantoms were developed. Nanoparticles of each sample were dispersed at different concentrations (10, 20, 30, 40 $\mu\text{g/ml}$) at 1% agarose gel in 10 ml tubes. The phantoms were scanned on a 3T Siemens clinical MRI system (MAGNETOM Prisma, Siemens Healthcare). T_2 and T_1 -weighted

Table 2

Adjusted parameters of temperature and pH to determine curcumin release from NCs using RSM, alpha is the distance of each axial point from the center point (mean of each parameter).

Symbol	Parameter	Units	Low level	High level	-Alpha	Alpha
A	Temperature (T)	$^{\circ}\text{C}$	38	55	34.4792	58.5208
B	pH		6	7.4	5.71005	7.68995

turbo spin-echo images (TSE) were obtained using the following parameters: TR = 3000 ms; TE = 10, 20, 30, 40, 50, 60, 70, 80, 90, 100 ms; Echo Train Length (ETL) = 10; Matrix = 256×256 ; Slice thickness = 3 mm.

2.5. In-vitro cell viability

Alamar blue assay was used to determine the effect of temperature-mediated release of curcumin and high temperature on the metabolic activity of MG-63 osteosarcoma cell line. The cells were cultured in a medium consisting of high glucose Dulbecco's Modified Eagle Medium (DMEM, Gibco, UK) and 1 mg/ml of the samples. The cells were cultured at 96 well plates for 24 h. Then different experimental groups of magnetic nanoparticles (i.e., NC and CurLNC) were added to each well plate followed by placing them in a temperature-controlled water bath at two different temperatures (i.e., 41°C and 45°C) for an hour (Fig. 5a). In the following, 440 mM dissolved resazurin (R7017, Sigma-Aldrich) in PBS, which was diluted ten times with DMEM medium, was added to the cells. After 2 h of incubation, the media was analyzed using Fluoroskan Ascent FL multiplate reader (Thermo LabSystems, Finland) at the wavelength of 570/620 nm. Three repetitions of each sample and one control group without particles were analyzed to extract the standard deviation and normalized data.

Live-dead staining assay was also used to qualitatively verify the cell viability of the nanocarriers. For this purpose, a staining kit (Molecular Probes, Thermo Scientific, US) after heat treating of cells was applied according to the manufacturer procedure. The fluorescence signal of live (green: 500–525 nm) and dead (red: 528–640 nm) cells was collected using a confocal laser microscope (CSLM- Leica SP8X, Germany) with hybrid detectors. Multiple images in the z-axis were stacked and merged using Leica LASX acquisition software to maximize the single intensity.

Caspase 3/7 assay (CellEvent™ Caspase-3/7 Green Detection Reagent) was used to stain the nucleus and quantify apoptotic cell death. In this regard, MG-63 cells were cultured and incubated in 96 well plate for 24 h. In the following, cells were incubated with curcumin loaded nanocarriers in the reagent diluted to a final concentration of 8 μM with the DMEM medium. The incubation was done in three temperatures of 37, 41 and 45°C . Then the media was analyzed using Fluoroskan Ascent FL multiplate reader (Thermo LabSystems, Finland) at the wavelength of 485/538 nm. The attached cells to the plate were also washed with PBS, and a confocal laser microscope (CSLM- Leica SP8X, Germany) was used to visualize the nucleus in the same excitation/emission wavelengths.

3. Results and discussion

Morphology, particle size, and dispersion of the nanoparticles were studied using TEM (Fig. 1a,b,c). showed the TEM images of SPION, SPION@OA-F127/F68 as nanocarrier (NC), and SPION@OA-F127/F68-Cur as curcumin loaded nanocarrier (CurLNC). The particle size was 9.4 ± 1.8 , 21.8 ± 3.3 , and 18.98 ± 4.6 nm for SPION, NC and CurLNC, respectively. Although coating bare SPION with branched molecules of oleic acid and pluronic increased the particles size due to the thickness of the polymeric shell, the particle size in NC and CurLNC was the same. The PDI was also calculated 0.04, 0.02 and 0.06 for SPION, NC and CurLNC, respectively which confirmed the monodispersity of the single particle size in all the samples. Reduced PDI after surface modification of the particles could be explained by steric stability of the particles, which rendered their appearance more distinguishable [38]. After loading curcumin, the colloidal stability of the particles was reduced due to the hydrophobic nature of curcumin, and consequently, PDI was increased [39]. The FTIR results represented the addition of the characteristic peaks of OA-F127/F68 in NC sample comparing to SPION and additional Curcumin peaks in CurLNC sample comparing to NC (Fig. 1d). The coating of OA-F127/F68 on the surface was discussed before [33]. The main specific peak of pluronic is C–O–C stretching vibrations peak at 1100 cm^{-1} . In CurLNC sample, the main distinguishing peaks of

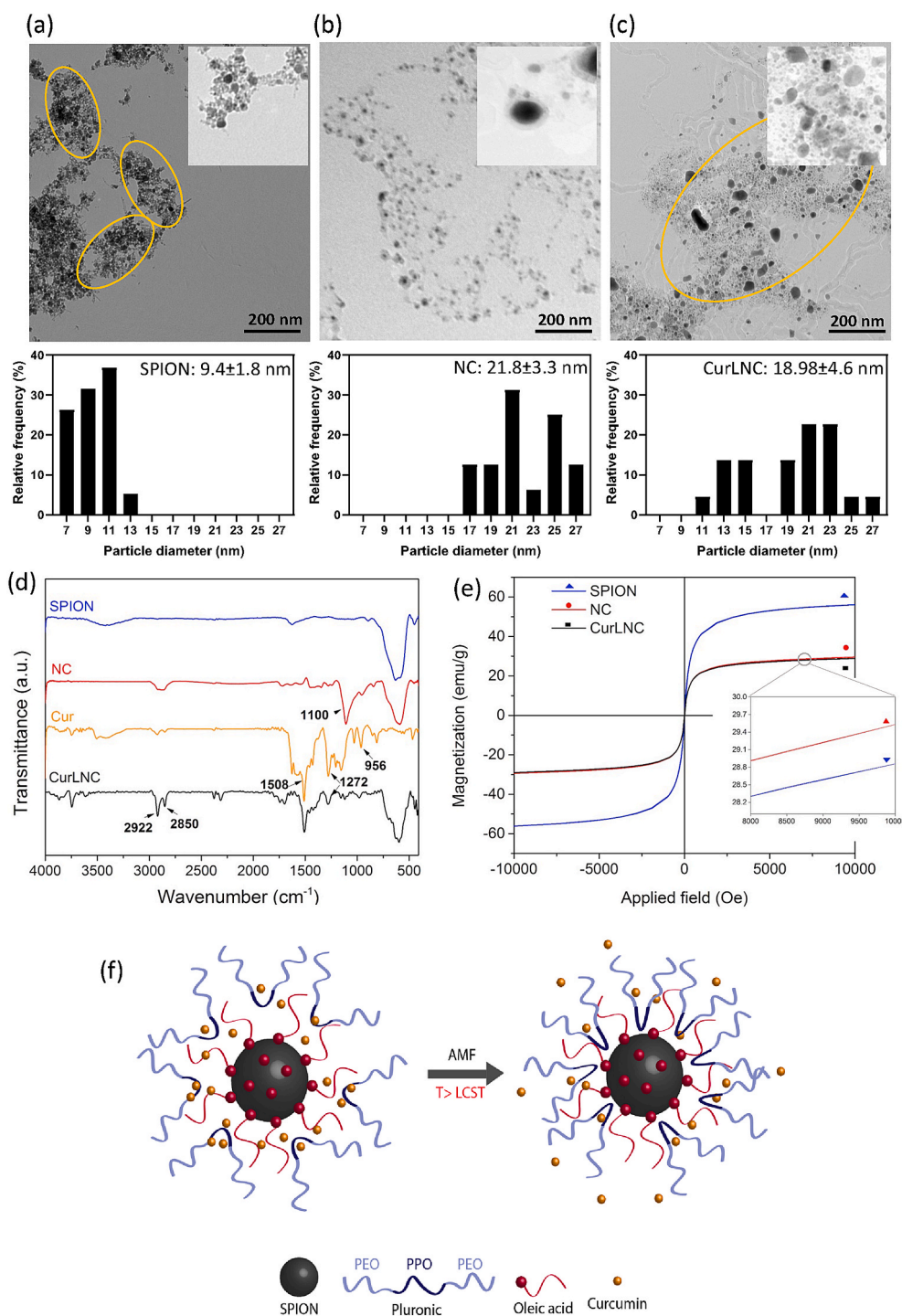


Fig. 1. The TEM micrograph and histogram of SPION (a), NC (b) and CurLNC (c) samples. The yellow circles demonstrated the nanoparticles aggregation in SPION and CurLNC whereas the NC nanoparticles were more monodispersed. The FTIR spectrum (d), and hysteresis loop extracted from VSM (e) for SPION, NC and CurLNC. The Schematic of CurLNC before (f) and after (g) applying AMF which modulates the drug release.

curcumin at 956, 1272, and 1508 cm^{-1} belong to benzoate *trans*-CH vibration, C–O, and C=O bonds [40]. The VSM diagrams in Fig. 1e showed the superparamagnetic behavior of the samples with the coercivity less than 1 Oe. Although the magnetic saturation of the bare SPION was about 56 emu/g, it decreased to around 30 emu/g for NC and CurLNC, which was mainly due to the spin-pinning of the domains on the surface of the particle by chemically absorbed functional groups [41]. Therefore, the non-significant effect of curcumin loading on the magnetic properties of the nanocarrier was due to the physical absorption of this small molecule in the polymeric shell. Fig. 1f and g

represented a schematic of CurLNC before and after the release of curcumin. The shrinkage of the polymeric layer stimulated by elevated temperature in the alternative magnetic field (AMF) was illustrated here which caused the curcumin release.

It was previously reported that elevated temperatures in the range of 30–60 °C after 1 h is achievable using magnetic nanoparticles at the dynamic electromagnetic field (300 kHz, 50–300 A) [42]. Fig. 2 a, b, c highlighted the hyperthermia effect of nanoparticles in different AMFs. having compared the rate of energy absorption in different samples, SAR was calculated, plotted (Fig. 2d) [43] and reflected an increase due to

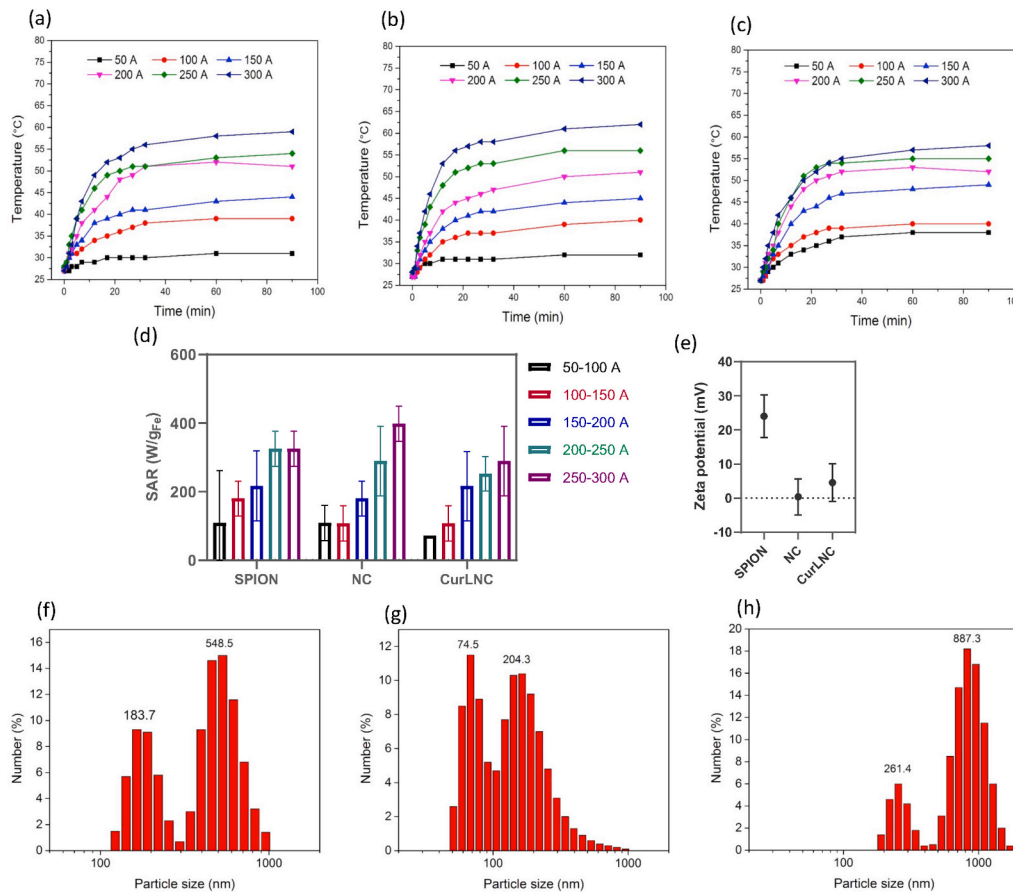


Fig. 2. Temperature versus time (a,b,c) and calculated SAR- error bars represent standard deviation of two replicates (d) at different AMFs for SPION, NC and CurLNC. zeta potential of SPION, NC and CurLNC at pH = 7 (e). The DLS reported size distribution of SPION (f), NC (g), and CurLNC (h) in the concentration of 1 mg/ml.

elevated current and magnetic field which is because of the higher thermal loss [37]. SAR of various magnetic colloids of Fe₃O₄ nanoparticles with different morphologies were previously reported in the same range [44].

The elevated temperature through magnetic nanoparticles in the AMFs can be created by three mechanisms of hysteresis loss, Brownian and Néel relaxation [42]. In the case of ultra-small superparamagnetic nanoparticles, the hysteresis loss contribution in the hyperthermia effect is not significant, and the effective relaxation time (τ) can be calculated using classic specific power absorption (SPA) model. According to this model, the effective relaxation time (τ) is made of Néel (τ_N) and Brownian (τ_B) relaxation times (equation (6) and (7)). Néel relaxation refers to the relaxation of the rotated spin in the particle and Brownian relaxation represents the mechanical relaxation of the rotated particle in the magnetic field.

$$\tau^{-1} = \tau_N^{-1} + \tau_B^{-1} \quad (6)$$

$$\tau_N = \tau_0 e^{\frac{KV_M}{k_B T}}, \quad \tau_B = \frac{3\eta V_h}{K_B T} \quad (7)$$

Where V_M and V_h the magnetic (particle) and hydrodynamic volumes, T temperature, η viscosity, K the magnetocrystalline anisotropy constant, K_B Boltzmann constant and the parameter τ_0 is attempt time with value of 10^{-9} – 10^{-11} s [45]. The maximum SPA happens at $\omega\tau = 1$; where ω is the frequency of the alternative magnetic field. In the condition of $\omega\tau < 1$, the relaxation time is less than time scale of magnetic field oscillation and if $\omega\tau > 1$, the oscillation of the magnetic field is too fast which prevents the relaxation of the particle [42]. Therefore, assuming $K = 2$ kJ/m³ for spherical magnetite, $T = 298$ K and $\eta = 8.9 \times 10^{-4}$ Pa s for

body simulating phantom, the optimum hydrodynamic diameter of the aggregated particles is approximately 100 nm. Therefore, different ultimate temperatures provided in AMF as NC > SPION > CurLNC can be explained by comparing their hydrodynamic diameter. DLS test displayed the distribution of the hydrodynamic diameter of the aggregated nanoparticles in 1 mg/ml concentration (Fig. 2f, g, h). Besides, the most important parameter to influence the SAR is magnetic anisotropy. Thus, the calculated values for all the samples are not significantly different [46].

The hydrodynamic diameter of NC was closer to this optimum diameter, and as a result, this sample provided higher temperatures. Applying polymeric shell reduced the hydrodynamic diameter (Fig. 2f, g,h), which was because of steric stabilization of the particles, whereas curcumin loading in the nanoparticles reduced the hydrophilicity and thereby increased the diameter of NCs aggregates [47]. Moreover, the temperature spectrum for different samples was directly correlated with the distribution of the hydrodynamic size. Notably, the DLS results also showed that the size distribution of the aggregated clusters was bimodal (Fig. 2f,g,h). Here, in addition to diffusion-limited cluster aggregation regime, small magnetic coercivity caused an interparticle force and consequently an extra regime of aggregation which can explain bimodal distribution [48]. The aggregates of SPIONs can be broken by surfactants such as pluronic (steric stability), and because of that, the average hydrodynamic diameter was reduced in NC. Zeta potential of the samples was investigated to confirm coating of pluronic on the surface (Fig. 2e). The zeta potential of SPION followed the reported values in the literature [49]. Surface charge of nanoparticles was reduced after coating of pluronic due to non-ionic nature of pluronic [50]. To select the optimum temperature for osteosarcoma therapy, the release study

and combinational effect of drug and hyperthermia on cell viability were studied.

Curcumin solution in acetone has a UV–Vis absorption at 419 nm, which is linearly correlated to its concentration [51]. Therefore, the calibration curve of curcumin in acetone was extracted in the range of 0–16 µg/ml. According to equations (4) and (5), the loading capacity and loading efficiency of curcumin in NCs were calculated 10.60% and 45.00%, respectively. The experiment to determine the release concentration was designed through Design Expert software. Using RSM, quadratic equation (8) was suggested to model curcumin release concentration from the carriers as a function of temperature and pH. This model was extracted from the release concentration as the response for 14 designed runs of the experiment.

$$\text{Release concentration } (\mu\text{g/ml}) = -423.91 + 18.06 \cdot T + 10.40 \cdot \text{pH} - 0.20 \cdot T^2 \quad (8)$$

The Analysis of variance (ANOVA) confirmed the model reliability in describing the response data. The applied regression with F-value of 12.08 and P-value of 0.005 is statistically significant. This model showed that with the temperature elevation up to 45 °C, the curcumin release reached its maximum point and then decreased in higher temperatures (Fig. 3a). As it was discussed before, the hydrophobicity of the pluronic chains is dependent on the temperature. The most known effect of increasing temperature on this tri-block copolymer is the sol-gel transition at LCST, which is 45 °C in this case. Although the pluronic chains are mostly hydrophilic, as the temperature increases up to LCST, the PPO blocks dehydrate and become more hydrophobic [52]. This transition leads to shrinkage of the pluronic shell and the release of the

absorbed drug. With the temperature elevation going on, even the PEO groups dehydrated, and the hydrophobicity increased [52]. Although earlier studies on sol-gel transition in pluronic showed that this transition is non-kinetic and happens all in the LCST, the concentration of the released drug here is not step-like but bell-like [33,53]. This finding is explained by the high affinity of hydrophobic aromatic rings in curcumin to the pluronic gel, which prevents the release of curcumin from the carrier [54]. In other words, the competition between pluronic shrinkage, which caused increased release and pluronic-curcumin interaction which caused reduced release, determined the maximum release concentration around LCST.

When closely examining the curves, increasing pH to 7.4 also led to enhancing the curcumin concentration in PBS media (Fig. 3b). Similarly, Nagy et al. [51] research provided evidence that the pH effect rendered the release of curcumin from polycaprolactone carriers due to the higher solubility of curcumin in higher pH aqueous media. Barick et al. [29] used pluronic P123 to stabilize magnetite nanoparticles and also deliver curcumin in a pH-sensitive manner. They showed that a decrease in pH leads to increased release due to the stretching of PEO blocks in a proton-concentrated solution. As they studied this system in the time frames of 5–50 h, apparently, the conformation transition of the molecule was implying a kinetic process that is less effective than the solubility effect in short periods of time. Notably, the 2D contour plot (Fig. 3c) and 3D response surface plot (Fig. 3d) illustrated the spontaneous effect of these two parameters on the release concentration where the maximum release (60.75 µM) was gained at 45.15 °C and pH of 7.4.

The T₂-weighted MR images of nanoparticle-loaded 1% agarose gel with different concentrations showed the functionality of the

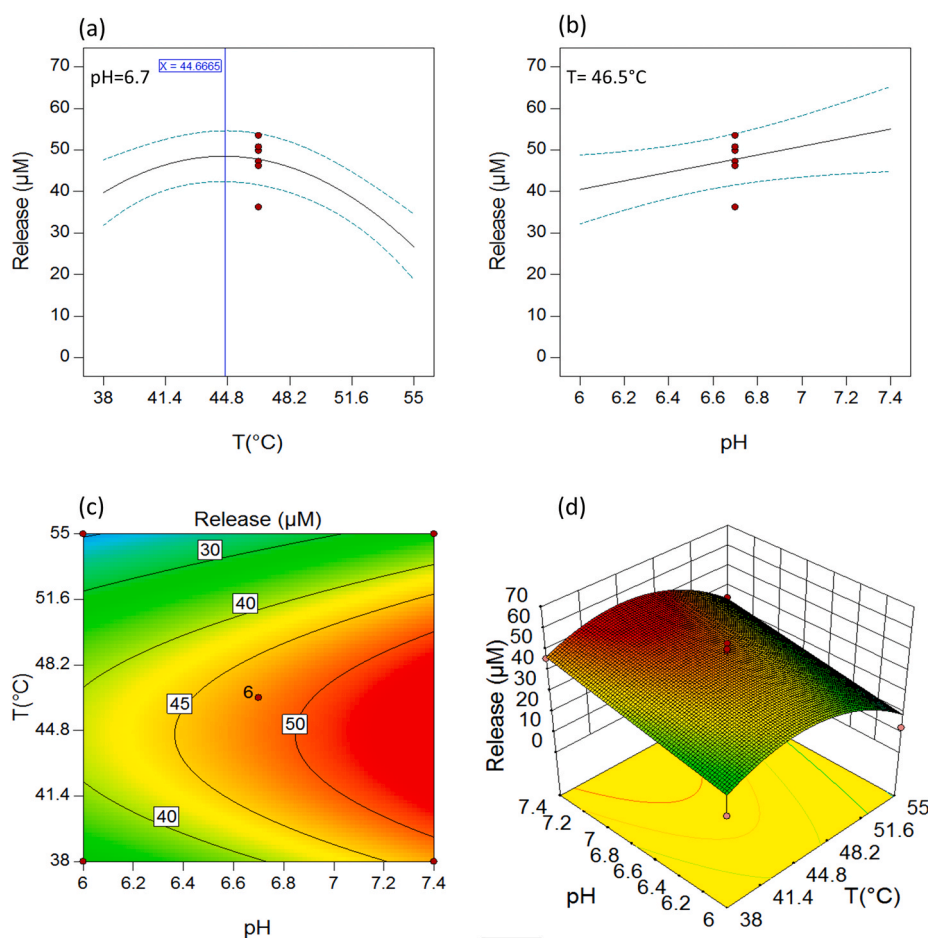


Fig. 3. Effect of temperature (a) and pH (b) on curcumin release at the center point value of the other parameter- dashed lines represent standard deviation according to 6 repeats of center point, 2D contour plot (c), and 3D response surface plot (d) of curcumin release versus temperature and pH.

therapeutic colloids as T_2 contrast agent (Fig. 4a). After the signal analysis, the longitudinal (R_1) and transverse (R_2) relaxation rates as a function of concentration were extracted according to the physical theory [55]. The slope of relaxation rate versus concentration (Fig. 4 b, c) is known as r_1 and r_2 , which determine the efficiency of the nanoparticles as a contrast agent. The values of r_2 , r_1 , and r_2/r_1 ratio were reported in Table 3, where r_2/r_1 in the range of [1–3,3–10], and >10 indicated positive, dual, and negative contrast agents, respectively [56]. The loaded and non-loaded carriers can be considered as negative contrast agents (Table 3), which can be used to monitor the nanocarriers position and the tumor size before and after the treatment. The trend of changing r_2 and r_2/r_1 ratio for the examined groups is NC > SPION > CurLNC. To explain this sequence, it is crucial to understand what determines the relaxation rate of protons in water molecules. According to equation (9), aggregated particles reduce the diffusion coefficient (D) and increase the diffusion time (τ_D). Where r is the radius of the spherical particles [57].

$$\tau_D = \frac{r^2}{D} \quad (9)$$

Considering $\Delta\omega$ as the root mean square of frequency shift at the particle surface, for short diffusion times ($\tau_D \ll 1/\Delta\omega$), $1/T_2$ depends on τ_D . This regime is called motional-averaging (MAR). As the τ_D increase, $1/T_2$ will also be affected and limited by echo time, called echo-limiting regime (ELR) [57]. The cumulative study by Young et al. [58] showed

that hydrodynamic diameter of less than 200 nm provides the maximum $1/T_2$ in the MAR regime. Although the hydrodynamic diameter of NC is close to this diameter, SPION and CurLNC aggregate size is practically pushing them into the ELR regime and reduce the $1/T_2$ and consequently r_2 .

To evaluate the independent effect of temperature and curcumin concentration on the cells, different groups such as control, NC, CurLNC and the medium containing curcumin concentrations (free drug) were chosen based on our released model (equation (8)). Then, these groups were prepared at 37, 41 and 45 °C (47, 57, 61 μ M), and cells were incubated in that for 1 h. The wells containing pure drug were incubated at 37 °C to eliminate the effect of temperature. The live-dead staining showed no significant difference between the control and NC groups at 37 °C and 41 °C; however, CurLNC group showed higher dead cells at these temperatures. At 45 °C, no live cells were observed in all the groups (Fig. 5b). The different curcumin concentrations didn't show any notable impact on killing cells at 37 °C, regardless of the temperature (Fig. 5c).

The Alamar blue activity confirmed the results of live-dead staining assay at different temperatures. The results showed significant difference between curcumin and CurLNC groups respect to the control group at 37 °C (Fig. 5d) rendering the effect of curcumin itself on cell metabolic activity. By increasing temperature to 41 °C, only CurLNC showed significant difference among all indicating a synergistic effect of temperature and curcumin concentration on cell metabolic activity (Fig. 5e).

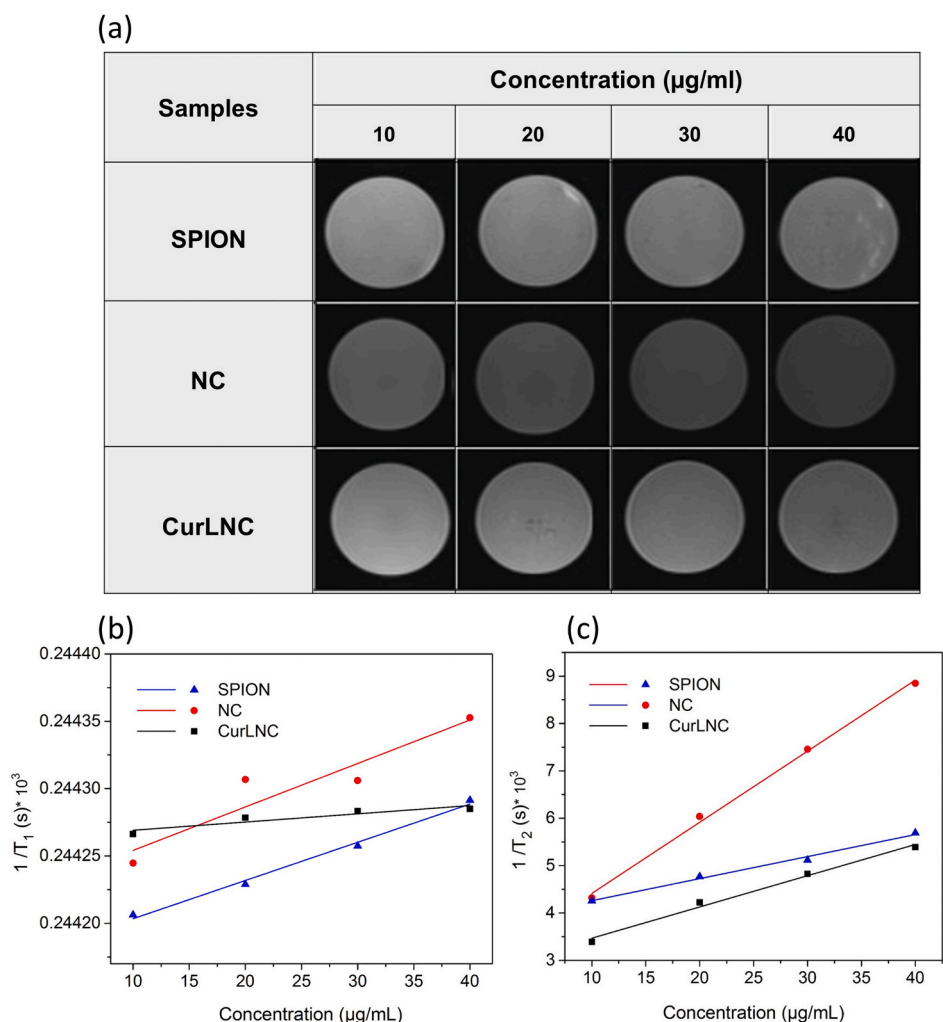


Fig. 4. T_2 weighted MR images of various concentrated nanoparticles in the phantom (a), Longitudinal R_1 (b), and transverse R_2 (c) Relaxation rates of SPION, NC, and CurLNC as a function of solid-phase concentration.

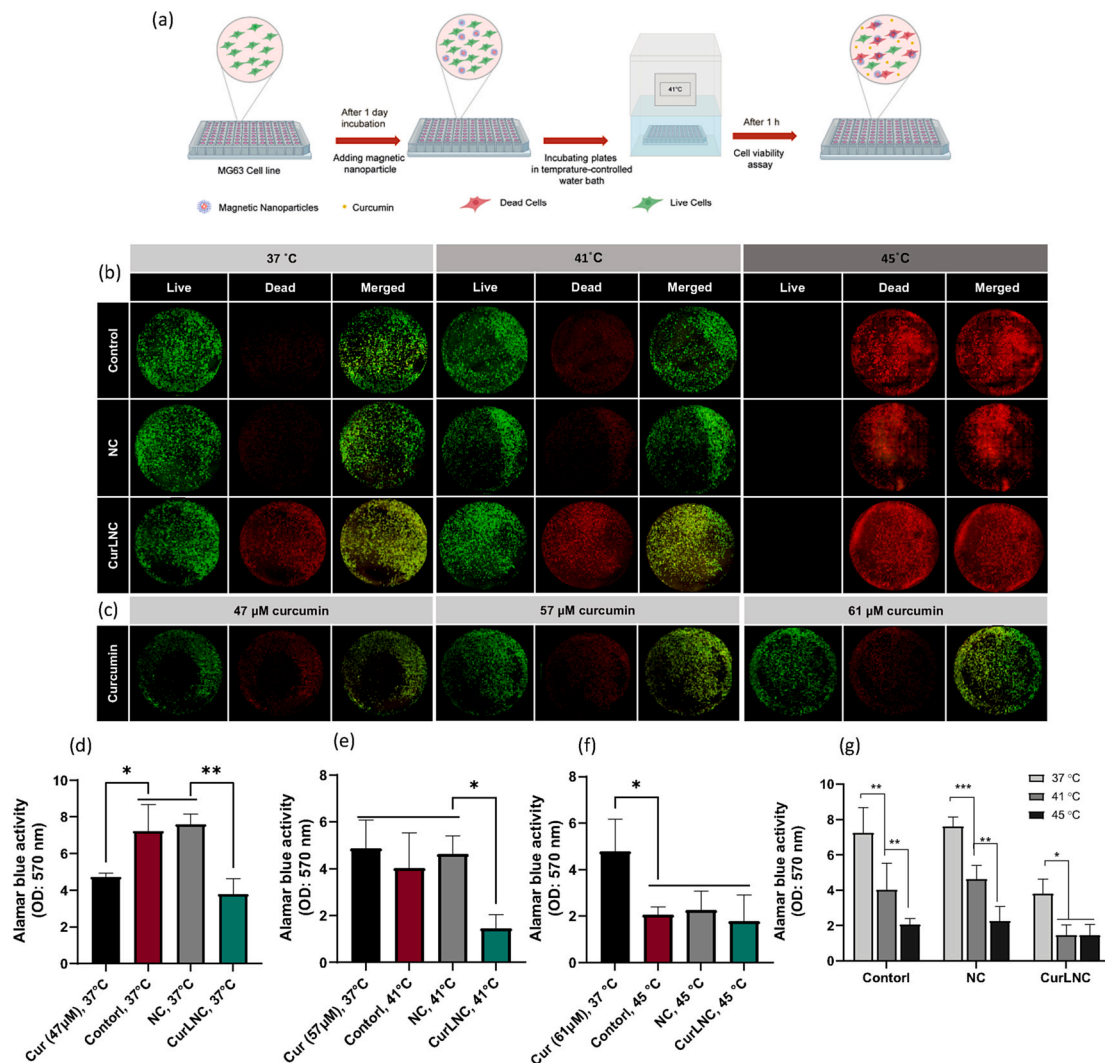


Fig. 5. Schematic of designed cell assay procedure to show the hyperthermia effect on cancer cells (a), CSLM images showing live/dead staining of MG-63 cancer cell lines at 37, 41 and 45 °C (b) estimated released concentrations of curcumin at 37, 41 and 45 °C, incubated at 37 °C (c) Alamar blue activity of MG-63 in the presence of NC and CurLNC at 37 °C (d), 41 °C (e), and 45 °C (f). Alamar blue activity of MG-63 for different experimental groups showing the effect of hyperthermia on cancer cells (f), error bars represent standard deviation of three replicates. *, $p < 0.05$; **, $p < 0.01$; ***, $p < 0.001$.

Table 3

Relaxometry results including longitudinal (r_1), transverse (r_2) relaxation and their ratio.

Sample	r_1 ($\mu\text{g/ml}^{-1} \cdot \text{s}^{-1}$)	r_2 ($\mu\text{g/ml}^{-1} \cdot \text{s}^{-1}$)	r_2/r_1
SPION	2.84 ± 0.18	46.51 ± 2.93	16.37 ± 1.46
NC	3.23 ± 0.82	150.10 ± 5.57	46.47 ± 11.92
CurLNC	6.12 ± 1.69	65.93 ± 4.53	10.79 ± 3.07

However, at higher temperature (i.e., 45 °C), no significant difference among all the groups was observed. Therefore, applying higher temperature (i.e., more than 41 °C) would exclude the effect of the drug on cell viability (Fig. 5f). Taken together, increasing temperature led to less metabolic activity (Fig. 5g). In particular, NC and CurLNC groups showed significant difference respect to the control at high temperature (i.e., 41 °C and 45 °C). However, no significant difference was observed between NC and CurLNC groups at 45 °C due to alleviation of drug effect at higher temperature (i.e., 45 °C).

Caspase 3/7 kit was used to quantify the cells death. Apoptosis or programmed cell-death is the preferred cell death pathway as it prevents inflammation and metastasis of the cancer cells [59,60]. Apoptosis has some biochemical signs which makes it distinguishable.

Caspase-mediated proteolysis of nuclear protein and degradation of the chromosomal DNA is one of the biochemical changes which can be quantified with the apoptosis caspase kits [60]. The reagent in this kit is DEVD peptide conjugated to a green detection dye. Although the reagent is intrinsically non-fluorescent, the dye would be cleaved and free to react with DNA and be fluorescent with caspase activation. Fig. 6a shows MG-63 cells incubated with CurLNC at three different temperatures of 37, 41 and 45 °C in caspase 3/7 kit reagent. At 37 °C, the nucleus was not stained. However, at 41 and 45 °C, the nucleus of cells was stained, which showed the activation of the effector caspase 3/7 [59].

The signal intensity of green dye was quantified using multiplate reader, which represents apoptosis death. Fig. 6b showed the fluorescent intensity of different groups at 41 and 45 °C compared to the control at 37 °C. The signal intensity was increased by temperature. Although the apoptosis signal was considerably higher at 45 °C comparing to 41 °C, the majority of cells at 41 °C got stained nucleus which confirms that extrinsic apoptosis pathway is activated in the cells. The larger number of dead cells and higher caspase activity at 45 °C exhibited the higher killing ability at this temperature.

To select the optimum temperature for cancer therapy using the curcumin loaded nanocarrier presented in this study, it is pivotal to prevent applied electromagnetic field heating the healthy tissues

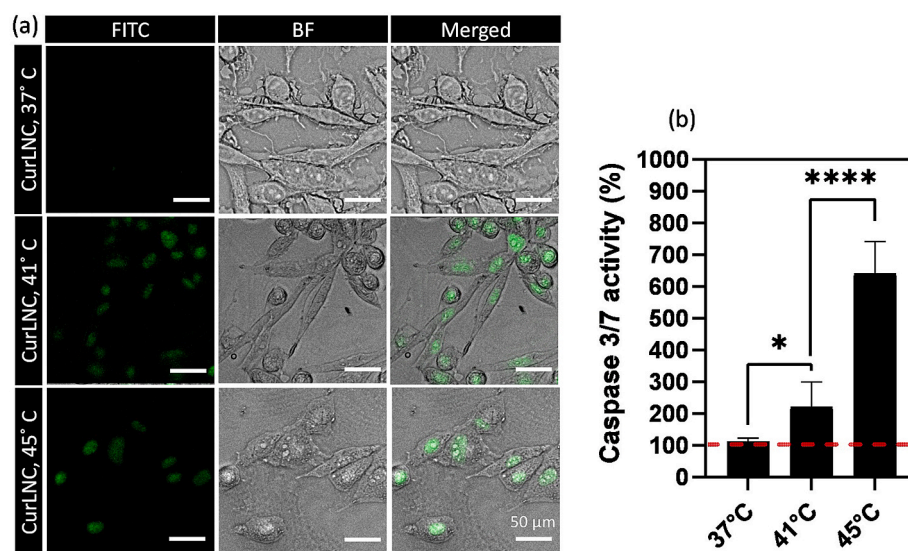


Fig. 6. CSLM and bright-field (BF) images showing cells incubated with CurLNC at 37, 41 and 45 °C in the presence of caspase 3/7 kit where the nucleus of apoptotic dead cells are stained green (a), quantified fluorescent intensity of green wavelength (normalized to the control group at 37 °C) which represents apoptosis, error bars represent standard deviation of three replicates (b), *, $p < 0.05$; ****, $p < 0.0001$.

through mild hyperthermia (temperatures lower than 43 °C) [61]. Interestingly, recent studies showed that mild hyperthermia is also able to trigger natural killer cells against tumors [61,62]. Therefore, a synergistic and non-intensive approach of mild hyperthermia (in 41 °C as the optimum temperature) and curcumin release will be recommended to treat osteosarcoma cancer cells.

4. Conclusions

Here, we proposed the simultaneous use of hyperthermia and controlled release of curcumin against bone tumors, which was verified through an *in vitro* study on MG-63 osteosarcoma cell line. The main aim of this research was to use mild hyperthermia (low frequency and low current) to prevent non-specific heating of the body tissues while amplifying the eradication of cancer cells by controlled delivery of curcumin. Magnetic nanocarriers with a thermo-responsive of the polymeric shell of pluronic F127/F68 were designed to control the release temperature, which was correlated with the LCST. An accessible temperature window with the loaded and non-loaded carriers was mainly dependent on alternative magnetic field parameters, saturation magnetization, and hydrodynamic diameter. To select the appropriate temperature for the hyperthermia cancer therapy, released drug concentration and cell viability tests were performed.

Although the highest caspase activation was monitored at 45 °C, stained nucleus and reduced metabolic activity of cells at 41 °C confirmed massive apoptosis at 41 °C. Thus, treatment at 41 °C is proposed to take advantage of non-aggressive mild hyperthermia condition. *In vitro* Alamar blue assay also confirmed the synergistic effect of curcumin and hyperthermia at 41 °C on osteosarcoma cell killing. Using 1 mg/ml of nanocarriers and applying an amperage of 100–150 A can provide this optimal condition for osteosarcoma therapy. Using these parameters, the temperature is stable during the treatment period and prevents any undesired hyperthermia. Furthermore, the nanocarriers used in this study showed the potential to be used as the negative MRI contrast agent to track residual cancer cells.

CRediT authorship contribution statement

A. Khodaei: Conceptualization, Investigation, Methodology, Formal analysis, Writing – original draft, Writing – review & editing. **F. Jahanmard:** Investigation, Methodology, Formal analysis, Writing –

original draft, Writing – review & editing. **H.R. Madaah Hosseini:** Conceptualization, Validation, Supervision, Resources, Funding acquisition, Writing – original draft. **R. Bagheri:** Conceptualization, Validation, Supervision, Resources, Funding acquisition, Writing – original draft. **A. Dabbagh:** Investigation, Resources. **H. Weinans:** Validation, Resources, Funding acquisition, Writing – original draft. **S. Amin Yavari:** Supervision, Validation, Resources, Funding acquisition, Writing – original draft, Writing – review & editing.

Declaration of competing interest

There is no conflict of interest.

Acknowledgments

None.

References

- [1] R. Eyre, R.G. Feltbower, E. Mubwandarikwa, T.O.B. Eden, R.J.Q. McNally, Epidemiology of bone tumours in children and young adults, *Pediatr. Blood Canc.* 53 (2009) 941–952, <https://doi.org/10.1002/pbc.22194>.
- [2] T.-T. Kuo, C.-H. Wang, J.-Y. Wang, H.-J. Chiou, C.-H. Fan, C.-K. Yeh, Concurrent osteosarcoma theranostic strategy using contrast-enhanced ultrasound and drug-loaded bubbles, *Pharmaceutics* 11 (2019) 223, <https://doi.org/10.3390/pharmaceutics11050223>.
- [3] D.D. Moore, H.H. Luu, Osteosarcoma (2014) 65–92, https://doi.org/10.1007/978-3-319-07323-1_4.
- [4] T.J. Webster, L. Sun, K. Chang, Short communication: selective cytotoxicity of curcumin on osteosarcoma cells compared to healthy osteoblasts, *Int. J. Nanomed.* (2014) 461, <https://doi.org/10.2147/IJN.S55505>.
- [5] D.K. Walters, R. Muff, B. Langsam, W. Born, B. Fuchs, Cytotoxic effects of curcumin on osteosarcoma cell lines, *Invest. N. Drugs* 26 (2008) 289–297, <https://doi.org/10.1007/s10637-007-9099-7>.
- [6] R. Taheri-Ledari, W. Zhang, M. Radmanesh, S.S. Mirmohammadi, A. Maleki, N. Cathcart, V. Kitaev, Multi-stimuli nanocomposite therapeutic: docetaxel targeted delivery and synergies in treatment of human breast cancer tumor, *Small* (2020) 2002733, <https://doi.org/10.1002/sml.202002733>.
- [7] A.L. Demain, P. Vaishnav, Natural products for cancer chemotherapy, *Microb. Biotechnol.* 4 (2011) 687–699, <https://doi.org/10.1111/j.1751-7915.2010.00221.x>.
- [8] V.S. Bollu, A.K. Barui, S.K. Mondal, S. Prashar, M. Fajardo, D. Briones, A. Rodríguez-Diéguez, C.R. Patra, S. Gómez-Ruiz, Curcumin-loaded silica-based mesoporous materials: synthesis, characterization and cytotoxic properties against cancer cells, *Mater. Sci. Eng. C* 63 (2016) 393–410, <https://doi.org/10.1016/j.msec.2016.03.011>.

- [9] A. Allegra, V. Innao, S. Russo, D. Gerace, A. Alonci, C. Musolino, Anticancer activity of curcumin and its analogues: preclinical and clinical studies, *Canc. Invest.* 35 (2017) 1–22, <https://doi.org/10.1080/07357907.2016.1247166>.
- [10] P. Angulo, G. Kaushik, D. Subramaniam, P. Dandawate, K. Neville, K. Chastain, S. Anant, Natural compounds targeting major cell signaling pathways: a novel paradigm for osteosarcoma therapy, *J. Hematol. Oncol.* 10 (2017) 10, <https://doi.org/10.1186/s13045-016-0373-z>.
- [11] S. Jin, H. Xu, J. Shen, X. Chen, H. Wang, J. Zhou, Apoptotic effects of curcumin on human osteosarcoma U2OS cells, *Orthop. Surg.* 1 (2009) 144–152, <https://doi.org/10.1111/j.1757-7861.2009.00019.x>.
- [12] P. Yadav, C. Zhang, A.K. Whittaker, K. Kailasam, A. Shanavas, Magnetic and photocatalytic curcumin bound carbon nitride nanohybrids for enhanced glioma cell death, *ACS Biomater. Sci. Eng.* 5 (2019) 6590–6601, <https://doi.org/10.1021/acsbomaterials.9b01224>.
- [13] A. Ashkbar, F. Rezaei, F. Attari, S. Ashkevarian, Treatment of breast cancer in vivo by dual photodynamic and photothermal approaches with the aid of curcumin photosensitizer and magnetic nanoparticles, *Sci. Rep.* 10 (2020) 21206, <https://doi.org/10.1038/s41598-020-78241-1>.
- [14] Y. Qiao, J. Wan, L. Zhou, W. Ma, Y. Yang, W. Luo, Z. Yu, H. Wang, Stimuli-responsive nanotherapeutics for precision drug delivery and cancer therapy, *Wiley Interdiscip. Rev. Nanomedicine Nanobiotechnology.* 11 (2019) e1527, <https://doi.org/10.1002/wnan.1527>.
- [15] H. Mok, M. Zhang, Superparamagnetic iron oxide nanoparticle-based delivery systems for biotherapeutics, *Expert Opin. Drug Deliv.* 10 (2013) 73–87, <https://doi.org/10.1517/17425247.2013.747507>.
- [16] L.M. De León-Rodríguez, A.F. Martins, M.C. Pinho, N.M. Rofsky, A.D. Sherry, Basic MR relaxation mechanisms and contrast agent design, *J. Magn. Reson. Imag.* 42 (2015) 545–565, <https://doi.org/10.1002/jmri.24787>.
- [17] H. Jeon, J. Kim, Y.M. Lee, J. Kim, H.W. Choi, J. Lee, H. Park, Y. Kang, I.-S. Kim, B.-H. Lee, A.S. Hoffman, W.J. Kim, Poly-paclitaxel/cyclodextrin-SPION nano-assembly for magnetically guided drug delivery system, *J. Contr. Release* 231 (2016) 68–76, <https://doi.org/10.1016/j.jconrel.2016.01.006>.
- [18] Arora Wahajuddin, Superparamagnetic iron oxide nanoparticles: magnetic nanoplateforms as drug carriers, *Int. J. Nanomed.* (2012) 3445, <https://doi.org/10.2147/IJN.S30320>.
- [19] P.J. Dobson, Nanoantenna Plasmon-Enhanced Spectroscopies for Biotechnological Applications, Marc Lamy de la Chapelle and Annemarie Pucci, 2015, <https://doi.org/10.1080/00107514.2015.1076049>.
- [20] S.S. Said, S. Campbell, T. Hoare, Externally addressable smart drug delivery vehicles: current technologies and future directions, *Chem. Mater.* 31 (2019) 4971–4989, <https://doi.org/10.1021/acs.chemmater.9b01798>.
- [21] M.M. Yallapu, S.F. Othman, E.T. Curtis, B.K. Gupta, M. Jaggi, S.C. Chauhan, Multi-functional magnetic nanoparticles for magnetic resonance imaging and cancer therapy, *Biomaterials* 32 (2011) 1890–1905, <https://doi.org/10.1016/j.biomaterials.2010.11.028>.
- [22] R. Bhandari, P. Gupta, T. Dziubla, J.Z. Hilt, Single step synthesis, characterization and applications of curcumin functionalized iron oxide magnetic nanoparticles, *Mater. Sci. Eng. C* 67 (2016) 59–64, <https://doi.org/10.1016/j.msec.2016.04.093>.
- [23] K.V. Jardim, A.F. Palomec-Garías, B.Y.G. Andrade, J.A. Chaker, S.N. Bão, C. Márquez-Beltrán, S.E. Moya, A.L. Parize, M.H. Sousa, Novel magneto-responsive nanoplateforms based on MnFe₂O₄ nanoparticles layer-by-layer functionalized with chitosan and sodium alginate for magnetic controlled release of curcumin, *Mater. Sci. Eng. C* 92 (2018) 184–195, <https://doi.org/10.1016/j.msec.2018.06.039>.
- [24] R. Basak, R. Bandyopadhyay, Encapsulation of hydrophobic drugs in pluronic F127 Micelles: effects of drug hydrophobicity, solution temperature, and pH, *Langmuir* 29 (2013) 4350–4356, <https://doi.org/10.1021/la304836e>.
- [25] H. Sun, Q. Meng, S. Tang, J. Su, Q. Yin, L. Chen, W. Gu, H. Yu, Z. Zhang, S. Wang, Y. Li, Inhibition of breast cancer metastasis by pluronic copolymers with moderate HLB, *Mol. Pharm.* (1979) 1–28.
- [26] N.U. Khaliq, D.Y. Park, B.M. Yun, D.H. Yang, Y.W. Jung, J.H. Seo, C.S. Hwang, S. H. Yuk, Pluronic: intelligent building units for targeted cancer therapy and molecular imaging, *Int. J. Pharm.* 556 (2019) 30–44, <https://doi.org/10.1016/j.ijpharm.2018.11.064>.
- [27] C. Farace, P. Sánchez-Moreno, M. Orecchioni, R. Manetti, F. Sgarrella, Y. Asara, J. M. Peula-García, J.A. Marchal, R. Madeddu, L.G. Delogu, Immune cell impact of three differently coated lipid nanocapsules: pluronic, chitosan and polyethylene glycol, *Sci. Rep.* 6 (2016) 18423, <https://doi.org/10.1038/srep18423>.
- [28] H.G. Kim, S.-H. Jo, S. Yeon, K.H. Kim, J.W. Chung, T.W. Park, Y. Byun, E.H. Lee, Y. I. Park, Y.W. Jung, Pluronic nanoparticles do not modulate immune responses mounted by macrophages, *Macromol. Res.* 21 (2013) 1355–1359, <https://doi.org/10.1007/s13233-013-1174-7>.
- [29] K.C. Barick, E. Ekta, S.L. Gawali, A. Sarkar, A. Kunwar, K.I. Priyadarsini, P. A. Hassan, Pluronic stabilized Fe₃O₄ magnetic nanoparticles for intracellular delivery of curcumin, *RSC Adv.* 6 (2016) 98674–98681, <https://doi.org/10.1039/C6RA21207G>.
- [30] E.C. Abenojar, S. Wickramasinghe, J. Bas-Concepcion, A.C.S. Samia, Structural effects on the magnetic hyperthermia properties of iron oxide nanoparticles, *Prog. Nat. Sci. Mater. Int.* 26 (2016) 440–448, <https://doi.org/10.1016/j.pnsc.2016.09.004>.
- [31] Y. Krupskaya, C. Mahn, A. Parameswaran, A. Taylor, K. Krämer, S. Hampel, A. Leonhardt, M. Ritschel, B. Büchner, R. Klingeler, Magnetic study of iron-containing carbon nanotubes: feasibility for magnetic hyperthermia, *J. Magn. Magn. Mater.* 321 (2009) 4067–4071, <https://doi.org/10.1016/j.jmmm.2009.08.005>.
- [32] P.C. Guillemin, L. Gui, O. Lorton, T. Zilli, L.A. Crowe, S. Desgranges, X. Montet, S. Terraz, R. Miralbell, R. Salomir, S. Boudabbous, Mild hyperthermia by MR-guided focused ultrasound in an ex vivo model of osteolytic bone tumour: optimization of the spatio-temporal control of the delivered temperature, *J. Transl. Med.* 17 (2019) 350, <https://doi.org/10.1186/s12967-019-2094-x>.
- [33] A. Khodaei, R. Bagheri, H.R. Madaah Hosseini, E. Bagherzadeh, RSM based engineering of the critical gelation temperature in magneto-thermally responsive nanocarriers, *Eur. Polym. J.* 120 (2019) 109197, <https://doi.org/10.1016/j.eurpolymj.2019.08.024>.
- [34] K.N. Clayton, J.W. Salameh, S.T. Wereley, T.L. Kinzer-Ursem, Physical characterization of nanoparticle size and surface modification using particle scattering diffusometry, *Biomicrofluidics* 10 (2016), 054107, <https://doi.org/10.1063/1.4962992>.
- [35] A. Dabbagh, B.J.J. Abdullah, N.H. Abu Kasim, C. Ramasindarum, Reusable heat-sensitive phantom for precise estimation of thermal profile in hyperthermia application, *Int. J. Hyperther.* 30 (2014) 66–74, <https://doi.org/10.3109/02656736.2013.854930>.
- [36] A. Dabbagh, Z. Hedayatnasab, H. Karimian, M. Sarraf, C.H. Yeong, H.R. Madaah Hosseini, N.H. Abu Kasim, T.W. Wong, N.A. Rahman, Polyethylene glycol-coated porous magnetic nanoparticles for targeted delivery of chemotherapeutics under magnetic hyperthermia condition, *Int. J. Hyperther.* 36 (2019) 104–114, <https://doi.org/10.1080/02656736.2018.1536809>.
- [37] Z. Hedayatnasab, A. Dabbagh, F. Abnisa, W.M.A. Wan Daud, Synthesis and in-vitro characterization of superparamagnetic iron oxide nanoparticles using a sole precursor for hyperthermia therapy, *Mater. Res. Bull.* 132 (2020) 110975, <https://doi.org/10.1016/j.materresbull.2020.110975>.
- [38] Y. Mohammad, A.B. Fallah, J.N.J. Reynolds, B.J. Boyd, S.B. Rizwan, Steric stabilisers govern the colloidal and chemical stability but not in vitro cellular toxicity of linoleylethanolamide cubosomes, *Colloids Surf. B Biointerfaces* 192 (2020) 111063, <https://doi.org/10.1016/j.colsurfb.2020.111063>.
- [39] C. Xu, S. Sun, Monodisperse magnetic nanoparticles for biomedical applications, *Polym. Int.* 56 (2007) 821–826, <https://doi.org/10.1002/pi.2251>.
- [40] P.R.K. Mohan, G. Sreelakshmi, C.V. Muraliedharan, R. Joseph, Water soluble complexes of curcumin with cyclodextrins: characterization by FT-Raman spectroscopy, *Vib. Spectrosc.* 62 (2012) 77–84, <https://doi.org/10.1016/j.vibspec.2012.05.002>.
- [41] K.J. Davies, S. Wells, S.W. Charles, The effect of temperature and oleate adsorption on the growth of maghemite particles, *J. Magn. Magn. Mater.* 122 (1993) 24–28, [https://doi.org/10.1016/0304-8853\(93\)91031-2](https://doi.org/10.1016/0304-8853(93)91031-2).
- [42] A.E. Deatsch, B.A. Evans, Heating efficiency in magnetic nanoparticle hyperthermia, *J. Magn. Magn. Mater.* 354 (2014) 163–172, <https://doi.org/10.1016/j.jmmm.2013.11.006>.
- [43] G. Cappiello, B. McGinley, M.A. Elahi, T. Drizdal, M.M. Paulides, M. Glavin, M. O'Halloran, E. Jones, Differential evolution optimization of the SAR distribution for head and neck hyperthermia, *IEEE Trans. Biomed. Eng.* 64 (2017) 1875–1885, <https://doi.org/10.1109/TBME.2016.2627941>.
- [44] P. Das, M. Colombo, D. Prosperi, Recent advances in magnetic fluid hyperthermia for cancer therapy, *Colloids Surf. B Biointerfaces* 174 (2019) 42–55, <https://doi.org/10.1016/j.colsurfb.2018.10.051>.
- [45] T.E. Torres, E. Lima, M.P. Calatayud, B. Sanz, A. Ibarra, R. Fernández-Pacheco, A. Mayoral, C. Marquina, M.R. Ibarra, G.F. Goya, The relevance of Brownian relaxation as power absorption mechanism in Magnetic Hyperthermia, *Sci. Rep.* 9 (2019) 3992, <https://doi.org/10.1038/s41598-019-40341-y>.
- [46] H. Khurshid, J. Alonso, Z. Nemati, M.H. Phan, P. Mukherjee, M.L. Fdez-Gubieda, J. M. Barandiarán, H. Srikanth, Anisotropy effects in magnetic hyperthermia: a comparison between spherical and cubic exchange-coupled Fe₃O₄ nanoparticles, *J. Appl. Phys.* 117 (2015) 17A337, <https://doi.org/10.1063/1.4919250>.
- [47] R. Mohammadi, J. Wassink, A. Amirfazli, Effect of surfactants on wetting of super-hydrophobic surfaces, *Langmuir* 20 (2004) 9657–9662, <https://doi.org/10.1021/la049268k>.
- [48] D. Asnaghi, M. Carpineti, M. Giglio, M. Sozzi, Coagulation kinetics and aggregate morphology in the intermediate regimes between diffusion-limited and reaction-limited cluster aggregation, *Phys. Rev.* 45 (1992) 1018–1023, <https://doi.org/10.1103/PhysRevA.45.1018>.
- [49] J. Gautier, E. Munnier, A. Paillard, K. Hervé, L. Douziech-Eyrolles, M. Soucé, P. Dubois, I. Chourpa, A pharmaceutical study of doxorubicin-loaded PEGylated nanoparticles for magnetic drug targeting, *Int. J. Pharm.* 423 (2012) 16–25, <https://doi.org/10.1016/j.ijpharm.2011.06.010>.
- [50] I. Pepić, A. Hafner, J. Lovrić, B. Pirkić, J. Filipović-Grcić, A nonionic surfactant/chitosan Micelle system in an innovative eye drop formulation, *J. Pharm. Sci.* 99 (2010) 4317–4325, <https://doi.org/10.1002/jps.22137>.
- [51] N.Z. Nagy, Z. Varga, J. Mihály, G. Kasza, B. Ivan, E. Kiss, Highly efficient encapsulation of curcumin into and pH-controlled drug release from poly(ϵ -caprolactone) nanoparticles stabilized with a novel amphiphilic hyperbranched polyglycerol, *Express Polym. Lett.* 14 (2020) 90–101, <https://doi.org/10.3144/expresspolymlett.2020.8>.
- [52] E.C. Rodrigues, M.A. Morales, S.N. De Medeiros, N.M. Suguhiro, Pluronic® coated sterically stabilized magnetite nanoparticles for hyperthermia applications, *J. Magn. Magn. Mater.* 416 (2016) 434–440, <https://doi.org/10.1016/j.jmmm.2016.05.033>.
- [53] A.M. Pragatheeswaran, S.B. Chen, Effect of chain length of PEO on the gelation and micellization of the pluronic F127 copolymer aqueous system, *Langmuir* 29 (2013) 9694–9701, <https://doi.org/10.1021/la401639g>.
- [54] P. Singla, O. Singh, S. Sharma, K. Betlem, V.K. Aswal, M. Peeters, R.K. Mahajan, Temperature-dependent solubilization of the hydrophobic antiepileptic drug lamotrigine in different pluronic Micelles—a spectroscopic, heat transfer method,

- small-angle neutron scattering, dynamic light scattering, and in vitro release study, *ACS Omega* 4 (2019) 11251–11262, <https://doi.org/10.1021/acsomega.9b00939>.
- [55] A. Khodaei, M. Malek, H.R.M. Hosseini, H. Delavari H, P. Vahdatkhah, A study on the concentration-dependent relaxometric transition in manganese oxide nanocolloid as MRI contrast agent, *ChemistrySelect* 4 (2019) 7596–7601, <https://doi.org/10.1002/slct.201901760>.
- [56] D. Zhu, F. Liu, L. Ma, D. Liu, Z. Wang, Nanoparticle-based systems for T1-weighted magnetic resonance imaging contrast agents, *Int. J. Mol. Sci.* 14 (2013) 10591–10607, <https://doi.org/10.3390/ijms140510591>.
- [57] R.A. Brooks, T2-shortening by strongly magnetized spheres: a chemical exchange model, *Magn. Reson. Med.* 47 (2002) 388–391, <https://doi.org/10.1002/mrm.10064>.
- [58] Q.L. Vuong, J.-F. Berret, J. Fresnais, Y. Gossuin, O. Sandre, A universal scaling law to predict the efficiency of magnetic nanoparticles as MRI T2-contrast agents, *Adv. Healthc. Mater.* 1 (2012) 502–512, <https://doi.org/10.1002/adhm.201200078>.
- [59] K. Matsuura, K. Canfield, W. Feng, M. Kurokawa, in: *Metabolic Regulation of Apoptosis in Cancer*, 2016, pp. 43–87, <https://doi.org/10.1016/bs.ircmb.2016.06.006>.
- [60] G. Häcker, The morphology of apoptosis, *Cell Tissue Res.* 301 (2000) 5–17, <https://doi.org/10.1007/s004410000193>.
- [61] J. Pan, Y. Xu, Q. Wu, P. Hu, J. Shi, Mild magnetic hyperthermia-activated innate immunity for liver cancer therapy, *J. Am. Chem. Soc.* 143 (2021) 8116–8128, <https://doi.org/10.1021/jacs.1c02537>.
- [62] X. Liu, J. Zheng, W. Sun, X. Zhao, Y. Li, N. Gong, Y. Wang, X. Ma, T. Zhang, L.-Y. Zhao, Y. Hou, Z. Wu, Y. Du, H. Fan, J. Tian, X.-J. Liang, Ferrimagnetic vortex nanoring-mediated mild magnetic hyperthermia imparts potent immunological effect for treating cancer metastasis, *ACS Nano* 13 (2019) 8811–8825, <https://doi.org/10.1021/acsnano.9b01979>.